Frustrated Further-Neighbor Antiferromagnetic and Electron-Hopping Interactions in the $d = 3$ tJ Model: Finite-Temperature Global Phase Diagrams from Renormalization-Group Theory

C. Nadir Kaplan,[1,2,3] A. Nihat Berker,[4,5,6] and Michael Hinczewski[6,7]
[1] *Department of Physics, Istanbul Technical University, Maslak 34469, Istanbul, Turkey,*
[2] *Department of Physics, Koç University, Sarıyer 34450, Istanbul, Turkey,*
[3] *Martin Fisher School of Physics, Brandeis University, Waltham, Massachusetts 02454, U.S.A.,*
[4] *Faculty of Engineering and Natural Sciences, Sabancı University, Orhanlı, Tuzla 34956, Istanbul, Turkey,*
[5] *Department of Physics, Massachusetts Institute of Technology, Cambridge, Massachusetts 02139, U.S.A.,*
[6] *Feza Gürsey Research Institute, TÜBITAK - Bosphorus University, Çengelköy 34684, Istanbul, Turkey and*
[7] *Department of Physics, Technical University of Münich, 85748 Garching, Germany*

The renormalization-group theory of the $d = 3$ tJ model is extended to further-neighbor antiferromagnetic or electron-hopping interactions, including the ranges of frustration. The global phase diagram of each model is calculated for the entire ranges of temperatures, electron densities, further/first-neighbor interaction-strength ratios. With the inclusion of further-neighbor interactions, an extremely rich phase diagram structure is found and is explained by competing and frustrated interactions. In addition to the τ_{tJ} phase seen in earlier studies of the nearest-neighbor $d = 3$ tJ model, the τ_{Hb} phase seen before in the $d = 3$ Hubbard model appears both near and away from half-filling.

PACS numbers: 71.10.Fd, 05.30.Fk, 64.60.De, 74.25.Dw

I. INTRODUCTION

The simplest model electron conduction model, including nearest-neighbor hopping on a lattice and on-site Coulomb repulsion, is the Hubbard model [1]. In the limit of very strong on-site Coulomb repulsion, second-order perturbation theory on the Hubbard model yields the tJ model [2, 3], in which sites doubly occupied by electrons do not exist. Studies of the Hubbard model [4] and of the tJ model [5], including spatial anisotropy [6] and quenched non-magnetic impurities [7] in good agreement with experiments, have shown the effectiveness of renormalization-group theory, especially in calculating phase diagrams at finite temperatures for the entire range of electron densities in $d = 3$. These calculations have revealed new phases, dubbed the τ phases, which occur only in these electronic conduction models under doping conditions. The telltale characteristics of the τ phases are, in contrast to all other phases of the systems, a non-zero electron-hopping probability at the largest length scales (at the renormalization-group thermodynamic-sink fixed points) and the divergence of the electron-hopping constant t under repeated rescalings. Furthermore, the phase diagram topologies, the doping ranges, and the contrasting quantitative τ and antiferromagnetic behaviors under quenched impurities [7] have been in agreement with experimental findings [8, 9]. A benchmark for this renormalization-group approach has also been established by a detailed and successful comparison, with the exact numerical results of the quantum transfer matrix method [10, 11], of the specific heat, charge susceptibility, and magnetic susceptibility in $d = 1$ calculated with our method.[12] Furthermore, results with this method have indicated that no finite-temperature phase transition occurs in the tJ model in $d = 1$. A phase separation at zero temperature has been found in $d = 1$ in Ref. [13]. Thus, the $d = 1$ tJ appears to have a first-order phase transition at zero temperature that disappears as soon as temperature is raised from zero, as in other $d = 1$ models such as the Ising and Blume-Capel models [14, 15]. A phase separation [16–18] occurs in $d = 2$ for low values of t/J, but not for $t/J > 0.24$.[5] In $d = 3$, a narrow phase separation occurs, as seen in the density - temperature phase diagrams below. Two distinct τ phases have been found in the Hubbard model [4], τ_{Hb} and τ_{tJ}, respectively occurring at weak and strong coupling. The calculated low-temperature behavior and critical exponent of the specific heat [4] have pointed to BCS-like and BEC-like behaviors, respectively. Only the τ_{tJ} phase was found in the tJ model.

The current work addresses the issue of whether both τ phases can be found in the tJ model, via the inclusion of further-neighbor antiferromagnetic (J_2) or further-neighbor electron hopping (t_2) interactions. We find that, depending on the temperature and doping level, the further-neighbor interactions may compete with the further-neighbor effects of the nearest-neighbor interactions, namely that frustration occurs as a function of temperature and doping level. This competition (or reinforcement) between the interactions of successive length scales underpins the calculated evolution of the phase diagrams. Global phase diagrams are obtained for the entire ranges of each type of further-neighbor interaction. With the inclusion of further-neighbor interactions, an extremely rich phase diagram structure is found and is explained by competing and frustrated interactions. Both τ_{Hb} and τ_{tJ} phases are indeed found to occur in the tJ model with the inclusion of these further-neighbor interactions. Furthermore, distinctive lamellar phase diagram structures of antiferromagnetism interestingly sur-

round the τ phases in the doped regions.

II. THE tJ HAMILTONIAN

On a d-dimensional hypercubic lattice, the tJ model is defined by the Hamiltonian

$$-\beta H = P\left[-t\sum_{\langle ij\rangle,\sigma}\left(c^\dagger_{i\sigma}c_{j\sigma}+c^\dagger_{j\sigma}c_{i\sigma}\right) -J\sum_{\langle ij\rangle}\mathbf{S}_i\cdot\mathbf{S}_j+V\sum_{\langle ij\rangle}n_in_j+\tilde{\mu}\sum_i n_i\right]P, \quad (1)$$

where $\beta = 1/k_BT$ and, with no loss of generality [5], $t \geq 0$ is used. Here $c^\dagger_{i\sigma}$ and $c_{j\sigma}$ are the creation and annihilation operators for an electron with spin $\sigma =\uparrow$ or $\downarrow$ at lattice site i, obeying anticommutation rules, $n_i = n_{i\uparrow}+n_{i\downarrow}$ are the number operators where $n_{i\sigma} = c^\dagger_{i\sigma}c_{i\sigma}$, and $\mathbf{S}_i = \sum_{\sigma\sigma'}c^\dagger_{i\sigma}\mathbf{s}_{\sigma\sigma'}c_{i\sigma'}$ is the single-site spin operator, with $\mathbf{s}$ the vector of Pauli spin matrices. The projection operator $P = \prod_i(1-n_{i\downarrow}n_{i\uparrow})$ projects out all states with doubly-occupied sites. The interaction constants t, J, V and $\tilde{\mu}$ correspond to electron hopping, nearest-neighbor antiferromagnetic coupling ($J > 0$), nearest-neighbor electron-electron interaction, and chemical potential, respectively. From rewriting the tJ Hamiltonian as a sum of pair Hamiltonians $-\beta H(i,j)$, Eq. (1) becomes

$$\begin{aligned}-\beta H =& \sum_{\langle ij\rangle}P\Big[-t\sum_\sigma\left(c^\dagger_{i\sigma}c_{j\sigma}+c^\dagger_{j\sigma}c_{i\sigma}\right) \\ &- J\mathbf{S}_i\cdot\mathbf{S}_j+Vn_in_j+\mu(n_i+n_j)\Big]P \quad (2)\\ \equiv& \sum_{\langle ij\rangle}\{-\beta H(i,j)\}\,,\end{aligned}$$

where $\mu = \tilde{\mu}/2d$. The standard tJ Hamiltonian is a special case of Eq. (2) with $V/J = 1/4$, which stems from second-order perturbation theory on the Hubbard model [2, 3].

III. RENORMALIZATION-GROUP TRANSFORMATION

A. $d = 1$ Recursion Relations

In $d = 1$, the Hamiltonian of Eq. (2) is

$$-\beta H = \sum_i\{-\beta H(i,i+1)\}\,. \quad (3)$$

A decimation eliminates every other one of the successive degrees of freedom arrayed in a linear chain, with the partition function being conserved, leading to a length rescaling factor $b = 2$. By neglecting the noncommutativity of the operators beyond three consecutive lattice sites, a trace over all states of even-numbered sites can be performed [19, 20],

$$\begin{aligned}\mathrm{Tr}_{\rm even}e^{-\beta H} &= \mathrm{Tr}_{\rm even}e^{\sum_i\{-\beta H(i,i+1)\}}\\ &= \mathrm{Tr}_{\rm even}e^{\sum_i{}^{\rm even}\{-\beta H(i-1,i)-\beta H(i,i+1)\}}\\ &\simeq \prod_i^{\rm even}\mathrm{Tr}_i e^{\{-\beta H(i-1,i)-\beta H(i,i+1)\}} = \prod_i^{\rm even}e^{-\beta' H'(i-1,i+1)}\\ &\simeq e^{\sum_i^{\rm even}\left\{-\beta' H'(i-1,i+1)\right\}} = e^{-\beta' H'}\,,\end{aligned} \quad (4)$$

where $-\beta' H'$ is the renormalized Hamiltonian. This approach, where the two approximate steps labeled with $\simeq$ are in opposite directions, has been successful in the detailed solutions of quantum spin [19–25] and electronic [4–7] systems. The anticommutation rules are correctly accounted within the three-site segments, at all successive length scales, in the iterations of the renormalization-group transformation.

The algebraic content of the decimation in Eq. (4) is

$$e^{-\beta' H'(i,k)} = \mathrm{Tr}_j e^{-\beta H(i,j)-\beta H(j,k)}, \quad (5)$$

where i, j, k are three consecutive sites of the unrenormalized linear chain. The renormalized Hamiltonian is given by

$$\begin{aligned}-\beta' H'(i,k) = P\Big[&-t'\sum_\sigma\left(c^\dagger_{i\sigma}c_{k\sigma}+c^\dagger_{k\sigma}c_{i\sigma}\right)\\ &- J'\mathbf{S}_i\cdot\mathbf{S}_k+V'n_in_k+\mu'(n_i+n_k)+G'\Big]P\,,\end{aligned} \quad (6)$$

where G' is the additive constant per bond, which is always generated in renormalization-group transformations, does not affect the flow of the other interaction constants, and is necessary in the calculation of expectation values. The values of the renormalized (primed) interaction constants appearing in $-\beta' H'$ are given by the recursion relations extracted from Eq. (5), which will be given here in closed form, while Appendix A details the derivation of Eq. (7) from Eq. (5):

$$\begin{aligned}t' &= \frac{1}{2}\ln\frac{\gamma_4}{\gamma_2}\,, \quad J' = \ln\frac{\gamma_6}{\gamma_7}\,, \quad V' = \frac{1}{4}\ln\frac{\gamma_1^4\gamma_6\gamma_7^3}{\gamma_2^4\gamma_4^4}\,,\\ \mu' &= \mu+\frac{1}{2}\ln\left(\frac{\gamma_2\gamma_4}{\gamma_1^2}\right), \quad G' = b^dG+\ln\gamma_1\,,\end{aligned} \quad (7)$$

$$\text{where} \qquad \gamma_1 = 1 + 2u^3 f(\frac{\mu}{2}) ,$$

$$\gamma_2 = uf\left(-\frac{\mu}{2}\right) + \frac{1}{2}u^2x^2 + \frac{3}{2}u^2vf\left(-\frac{J}{8} + \frac{V}{2} + \frac{\mu}{2}\right) ,$$

$$\gamma_4 = 1 + \frac{3}{2}u^2v^2 + \frac{1}{2}u^2xf\left(\frac{3J}{8} + \frac{V}{2} + \frac{\mu}{2}\right) ,$$

$$\gamma_6 = 2v^3x + xf\left(-\frac{3J}{8} - \frac{V}{2} - \frac{\mu}{2}\right) ,$$

$$\gamma_7 = \frac{2}{3}vx^3 + \frac{4}{3}v^4 + vf\left(\frac{J}{8} - \frac{V}{2} - \frac{\mu}{2}\right) , \qquad (8)$$

$$\text{and} \qquad v = \exp\left(-J/8 + V/2 + \mu/2\right) ,$$

$$x = \exp\left(3J/8 + V/2 + \mu/2\right) , \quad u = \exp\left(\mu/2\right) ,$$

$$f(A) = \cosh\sqrt{2t^2 + A^2} + \frac{A}{\sqrt{2t^2 + A^2}} \sinh\sqrt{2t^2 + A^2} . \qquad (9)$$

B. $d > 1$ Recursion Relations

The Migdal-Kadanoff renormalization-group procedure generalizes our transformation to $d > 1$ through a bond-moving step [26, 27]. Eq. (7) can be expressed as a mapping of interaction constants $\mathbf{K} = \{G, t, J, V, \mu\}$ onto renormalized interaction constants, $\mathbf{K'} = \mathbf{R}(\mathbf{K})$. The Migdal-Kadanoff procedure strengthens by a factor of b^{d-1} the bonds of linear decimation, to account for a bond-moving effect [26, 27]. The resulting recursion relations for $d > 1$ are,

$$\mathbf{K'} = b^{d-1}\mathbf{R}(\mathbf{K}), \qquad (10)$$

which explicitly are

$$t' = \frac{b^{d-1}}{2}\ln\frac{\gamma_4}{\gamma_2}, J' = b^{d-1}\ln\frac{\gamma_6}{\gamma_7}, V' = \frac{b^{d-1}}{4}\ln\frac{\gamma_1^4\gamma_6\gamma_7^3}{\gamma_2^4\gamma_4^4},$$

$$\mu' = b^{d-1}\mu + \frac{b^{d-1}}{2}\ln\left(\frac{\gamma_2\gamma_4}{\gamma_1^2}\right), G' = b^dG + b^{d-1}\ln\gamma_1. \qquad (11)$$

This approach has been successfully employed in studies of a large variety of quantum mechanical and classical (*e.g.,* references in [4]) systems.

C. Calculation of Phase Diagrams and Expectation Values

The global flows of Eq. (10), controlled by stable and unstable fixed points, yield the phase diagrams in temperature versus chemical potential [28]: The basin of attraction of each fixed point corresponds to a single thermodynamic phase or to a single type of phase transition, according to whether the fixed point is completely stable (a phase sink) or unstable. Eigenvalue analysis of the recursion matrix at an unstable fixed point determines the order and critical exponents of the phase transitions at the corresponding basin.

Phase	Interaction constants at sink			
	t	μ	J	V
d (dilute disordered)	0	$-\infty$	0	0
D (dense disordered)	0	∞	0	0
AF (antiferromagnetic)	0	∞	$-\infty$	$-\infty$ $\frac{V}{J} \to \frac{1}{4}$
τ_{tJ} (BEC-like superconductor)	∞ $\frac{t}{\mu} \to 1$	∞	∞ $\frac{J}{\mu} \to 2$	$-\infty$ $\frac{V}{J} \to -\frac{3}{4}$
τ_{Hb} (BCS-like superconductor)	$-\infty$ $\frac{t}{\mu} \to -1$	∞	$-\infty$ $\frac{J}{\mu} \to -2$	$-\infty$ $\frac{V}{J} \to \frac{1}{4}$

TABLE I: Interaction constants at the phase sinks.

Table I gives the interaction constants t, J, V, μ at the tJ model phase sinks. The τ_{tJ} and τ_{Hb} phases are the only regions where the electron-hopping term t does not renormalize to zero at the phase sinks. On the contrary, in these phases, $t \to \infty$ and $t \to -\infty$, respectively.

To compute temperature versus electron-density (doping) phase diagrams, thermodynamic densities are calculated by summing along entire renormalization-group flow trajectories.[29] A density, namely the expectation value of an operator in the Hamiltonian, is given by

$$M_\alpha = \frac{1}{Nd}\frac{\partial \ln Z}{\partial K_\alpha} , \qquad (12)$$

where K_α is an element of $\mathbf{K} = \{K_\alpha\}$, Z is the partition function, and N is the number of lattice sites. The recursion relations for densities are

$$M_\alpha = b^{-d}\sum_\beta M'_\beta T_{\beta\alpha} , \quad \text{where} \qquad T_{\beta\alpha} \equiv \frac{\partial K'_\beta}{\partial K_\alpha} . \qquad (13)$$

In terms of the density vector $\mathbf{M} = \{M_\alpha\}$ and the recursion matrix $\mathbf{T} = \{T_{\beta\alpha}\}$,

$$\mathbf{T} = \begin{pmatrix} b^d & \frac{\partial G'}{\partial t} & \frac{\partial G'}{\partial J} & \frac{\partial G'}{\partial V} & \frac{\partial G'}{\partial \mu} \\ 0 & \frac{\partial t'}{\partial t} & \frac{\partial t'}{\partial J} & \frac{\partial t'}{\partial V} & \frac{\partial t'}{\partial \mu} \\ 0 & \frac{\partial J'}{\partial t} & \frac{\partial J'}{\partial J} & \frac{\partial J'}{\partial V} & \frac{\partial J'}{\partial \mu} \\ 0 & \frac{\partial V'}{\partial t} & \frac{\partial V'}{\partial J} & \frac{\partial V'}{\partial V} & \frac{\partial V'}{\partial \mu} \\ 0 & \frac{\partial \mu'}{\partial t} & \frac{\partial \mu'}{\partial J} & \frac{\partial \mu'}{\partial V} & \frac{\partial \mu'}{\partial \mu} \end{pmatrix} , \qquad (14)$$

Eq. (13) simply is

$$\mathbf{M} = b^{-d}\mathbf{M'} \cdot \mathbf{T} . \qquad (15)$$

At a fixed point, the density vector $M_\alpha = M'_\alpha \equiv M^*_\alpha$ is the left eigenvector, with eigenvalue b^d, of the fixed-point

recursion matrix $\mathbf{T}^*$ (Table II). For non-fixed-points, iterating Eq. (15) n times,

$$\mathbf{M} = b^{-nd}\mathbf{M}^{(n)} \cdot \mathbf{T}^{(n)} \cdot \mathbf{T}^{(n-1)} \cdot \cdots \cdot \mathbf{T}^{(1)} , \qquad (16)$$

where, for n large enough, the trajectory arrives as close as desired to a completely stable (phase-sink) fixed point and $\mathbf{M}^{(n)} \simeq \mathbf{M}^*$. The latter density vector $\mathbf{M}^*$ is the left eigenvector of the recursion matrix with eigenvalue b^d. When two such density vectors exist, the two branches of the phase separation of a first-order phase transition are obtained [29, 30], as illustrated with the phase separations found below.

Phase sinks	Expectation values at sink			
	$\sum_\sigma \langle c^\dagger_{i\sigma} c_{j\sigma} + c^\dagger_{j\sigma} c_{i\sigma} \rangle$	$\langle n_i \rangle$	$\langle \mathbf{S}_i \cdot \mathbf{S}_j \rangle$	$\langle n_i n_j \rangle$
d	0	0	0	0
D	0	1	0	1
AF	0	1	$\frac{1}{4}$	1
τ_{tJ}	$-\frac{2}{3}$	$\frac{2}{3}$	$-\frac{1}{4}$	$\frac{1}{3}$
τ_{Hb}	0.664	0.668	0.084	0.336

TABLE II: Expectation values at the phase sinks. The expectation values at a sink epitomize the expectation values throughout its corresponding phases, because, as explained in Sec. IIIC, the expectation values at the phase sink underpin the calculation of the expectation values throughout the corresponding phase which is constituted from the basin of attraction of the sink.

IV. FURTHER-NEIGHBOR INTERACTIONS, TEMPERATURE- AND DOPING-DEPENDENT FRUSTRATION AND GLOBAL PHASE DIAGRAMS

For the results presented below, we use the theoretically and experimentally dictated initial conditions of $V/J = 1/4$ and $t/J = 2.25$.

The details of the thermodynamic phases found in this work, listed in Tables I and II, have been discussed previously within context of the nearest-neighbor tJ [5–7] and, for the τ_{Hb} phase, Hubbard [4] models. The τ_{Hb} phase is seen here in the tJ model with the inclusion of the further-neighbor antiferromagnetic or electron-hopping interaction. Suffice it to recall here that the τ phases are the only phases in which: (1) the electron-hopping strength does not renormalize to zero, but to infinity; (2) the electron density does not renormalize to complete emptiness or complete filling, but to partial emptiness/filling, leaving room for electron/hole conductivity; (3) the nearest-neighbor electron occupation probability does not renormalize to zero or unity, again leaving room for conductivity at the largest length scales; (4) the electron-hopping expectation value is non-zero at the largest length scales; (5) the experimentally observed chemical potential shift as a function of doping occurs

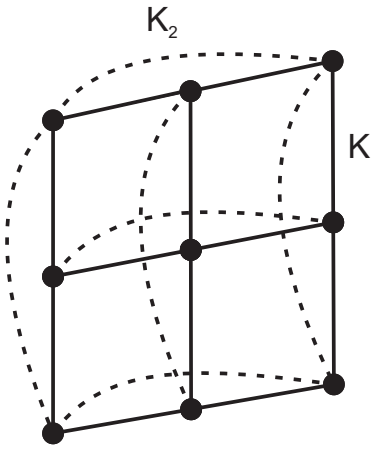

FIG. 1: Construction of the further-neighbor models. Part of a single plane of the three-dimensional model studied here is shown.

[6]; and (6) a low level ($\sim 6\%$) of quenched non-magnetic impurities causes total disappearance, in contrast to the antiferromagnetic phase ($\sim 40\%$ for total disappearance) [7], again as seen experimentally. The low-temperature behavior and critical exponent of the specific heat [4] have pointed to BCS-like and BEC-like behaviors for the τ_{Hb} and τ_{tJ} phases, respectively.

The only approximations in obtaining the results below are the Suzuki-Takano and Migdal-Kadanoff procedures, explained above in Secs. IIIA and IIIB respectively. There are no further assumptions in Secs.IVA and IVB below.

A. The t_2 Model

The t_2 model includes further-neighbor electron-hopping interaction, as shown in Fig. 1. The three-site Hamiltonian, between the lattice nodes at the lowest length scale, has the form:

$$\begin{aligned} -\beta H(i,j,k) = &- \beta H(i,j) - \beta H(j,k) \\ &- t_2 \sum_\sigma \left(c^\dagger_{i\sigma} c_{k\sigma} + c^\dagger_{k\sigma} c_{i\sigma} \right) , \end{aligned} \qquad (17)$$

where $-\beta H(i,j)$ is given in Eq. (2), so that the first equation of Eq. (7) gets modified as

$$t' = \frac{1}{2} \ln \frac{\gamma_4}{\gamma_2} + t_2 , \qquad (18)$$

only for the first renormalization. Thus, for $d = 3$, the first equation of Eq. (11) gets modified as

$$t' = 2 \ln \frac{\gamma_4}{\gamma_2} + 4\, t_2 , \qquad (19)$$

only for the first renormalization. Thus, the hopping-strength t_2 contributes to the first renormalization, but

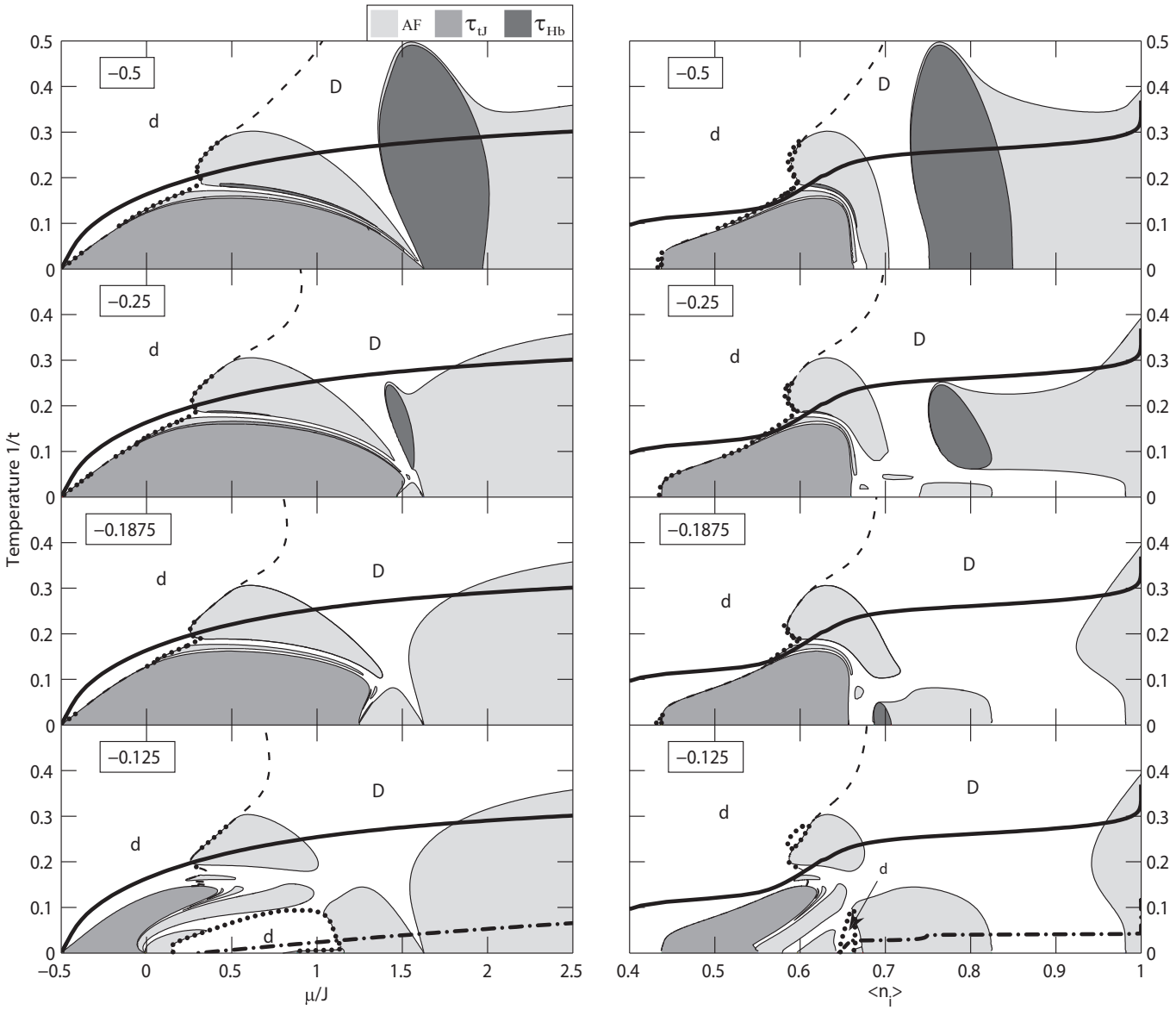

FIG. 2: Global phase diagram of the further-neighbor t_2 model for $t/J = 2.25$ in temperature vs. chemical potential (first column) and, correspondingly, temperature versus electron density (second column). The relation $t/J = 2.25$ is used for all renormalization-group trajectory initial conditions. The t_2/t values are given in boxes. The dilute disordered (d), dense disordered (D), antiferromagnetic AF (lightly colored), τ_{tJ} (medium colored), and τ_{Hb} (darkly colored) phases are seen. Second-order phase transitions are drawn with full curves, first-order transitions with dotted curves. Phase separation occurs between the dense (D) and dilute (d) disordered phases, in the unmarked areas within the dotted curves in the electron density vs. temperature diagrams. These areas are bounded, on the right and and the left, by the two branches of phase separation densities, evaluated by renormalization-group theory as explained in Sec.IIIC. Note that these coexistence regions between dense (D) and dilute (d) disordered phases are very narrow. Dashed curves are not phase transitions, but disorder lines between the dense and dilute disordered phases. As explained in the text, on each side of the thick full curves (not a phase boundary), the further-neighbor electron hopping affects the τ phases oppositely. On the dash-dotted curve (also not a phase boundary; overlaps, for $t_2/t = 0$, with the thick full curve) electron hopping in the system is frustrated.

is not regenerated by this first renormalization. Note that the quantitative memory of the further-neighbor interaction is kept in all subsequent renormalization-group steps, as the flows are modified by the different values of the first-renormalized interactions due to the effect of the further-neighbor interaction. The subsequent global renormalization-group flows are in the space of t, J, V, μ, as is the case in position-space renormalization-group treatments [31–33] using a prefacing transformation. Which surfaces in this large (4-dimensional) flow space of t, J, V, μ are accessed is controlled by the original further-neighbor interaction. Thus, the further-neighbor

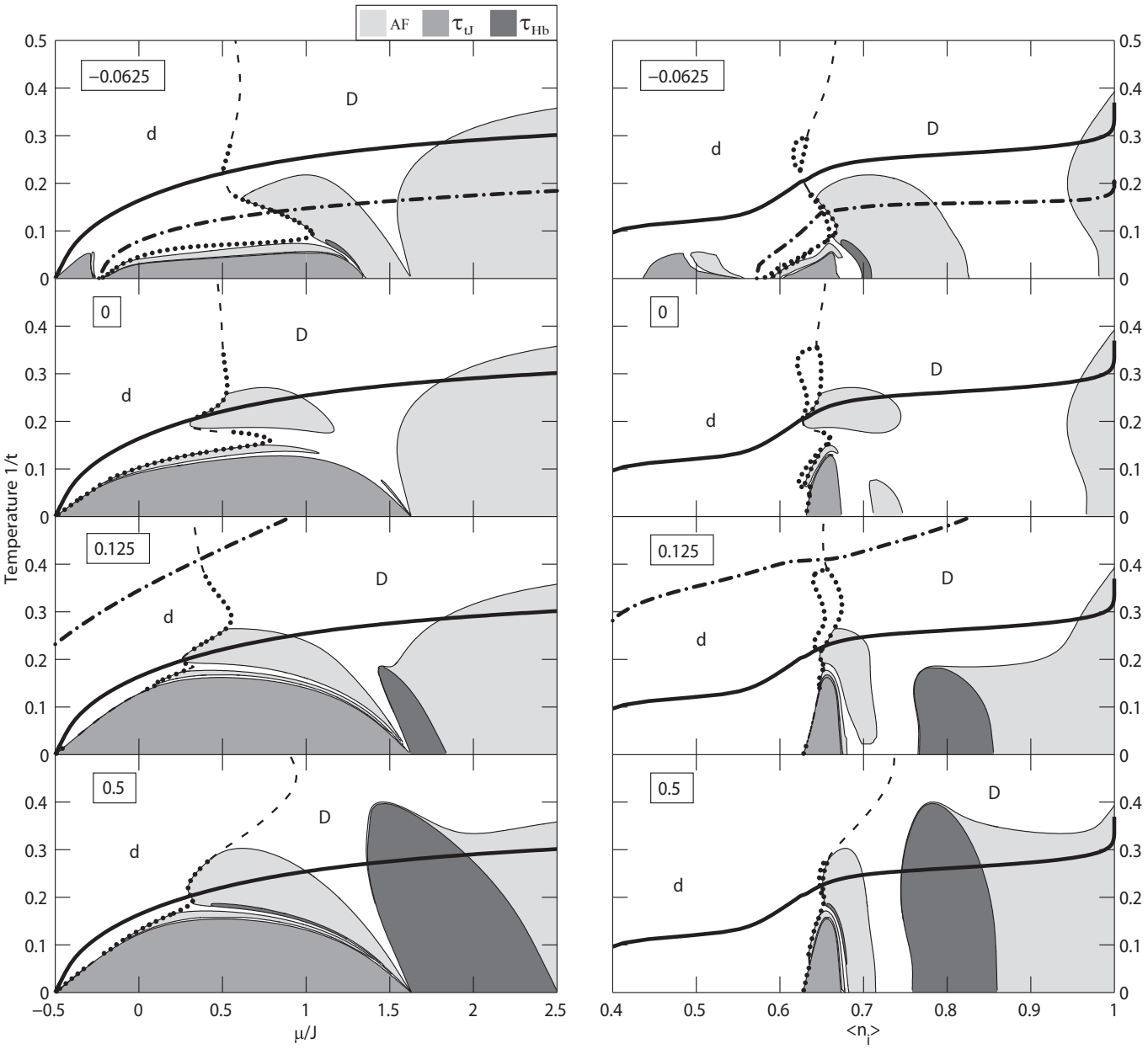

FIG. 3: The continuation of the global phase diagram in Fig. 2.

interaction t_2 shifts the value of t' obtained after the first renormalization-group transformation, as dictated by the physical model (Fig.1). Since the value of the first-renormalized t' in the absence of t_2 already has a complicated dependence on the unrenormalized temperature and electron density, the variety of phase diagrams is obtained. Indeed, the effect of the further-neighbor interaction is dependent on the electron density, temperature, and other interactions in the system, due to the presence of the first-term in Eq. (19), which is the key to the resulting spectacularly different phase diagrams as the further-neighbor interaction is varied. (1) If the two terms in Eq. (18) are of the same sign, the nearest-neighbor and further-neighbor electron hopping terms of the original system reinforce each other and the τ phases are enhanced. (2) If the two terms are of opposite signs, the nearest-neighbor and further-neighbor electron hopping terms of the original system compete with each other and, with the introduction of further-neighbor electron hopping, the τ phases are initially suppressed, but enhanced as further-neighbor hopping becomes dominant. The two regimes (1) and (2) are separated by the thick full lines in the phase diagrams in Figs. 2 and 3. In the case (2) of opposite signs, when the two terms cancel out each other, the system is frustrated, in which case, after the first renormalization, there is no electron hopping in the system. Since this condition is closed under renormalization, both on physical grounds and of course

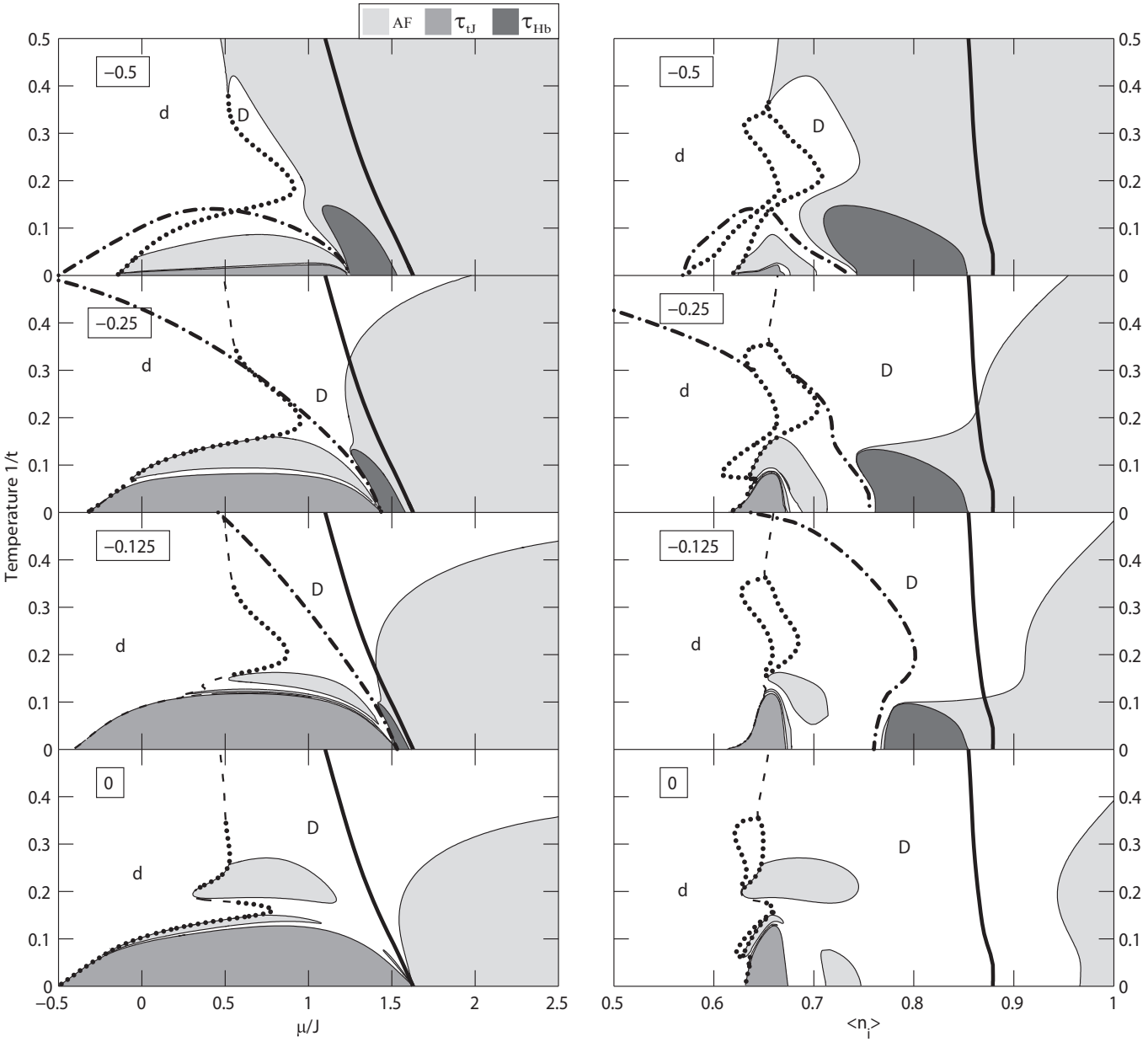

FIG. 4: Global phase diagrams of the further-neighbor J_2 model for $t/J = 2.25$ in temperature vs. chemical potential (first column) and, correspondingly, temperature versus electron density (second column). The relation $t/J = 2.25$ is used for all renormalization-group trajectory initial conditions. The J_2/J values are given in boxes. The dilute disordered (d), dense disordered (D), antiferromagnetic AF (lightly colored), τ_{tJ} (medium colored), and τ_{Hb} (darkly colored) phases are seen. Second-order phase transitions are drawn with full curves, first-order transitions with dotted curves. Phase separation occurs between the dense (D) and dilute (d) disordered phases, in the unmarked areas within the dotted curves in the electron density vs. temperature diagrams. These areas are bounded, on the right and and the left, by the two branches of phase separation densities, evaluated by renormalization-group theory as explained in Sec.IIIC. Note that these coexistence regions between dense (D) and dilute (d) disordered phases are very narrow. Dashed curves are not phase transitions, but disorder lines between the dense and dilute disordered phases. As explained in the text, on each side of the thick full curves (not a phase boundary), the further-neighbor interaction affects the antiferromagnetic phase oppositely. On the dash-dotted curve (also not a phase boundary; overlaps, for $J_2/J = 0$, with the thick full curve), antiferromagnetism in the system is frustrated.

in our recursion relations (Eq. (7)), no τ phase can occur in such a system. The dash-dotted curves in Figs. 2 and 3 indeed show such systems. These competition, reinforcement, and frustration effects are temperature and doping dependent. These, and all other physical effects, do not depend on the sign of nearest-neighbor t of the original unrenormalized system, due to the symmetry of hypercubic lattices [5] and as seen in Eq. (9).

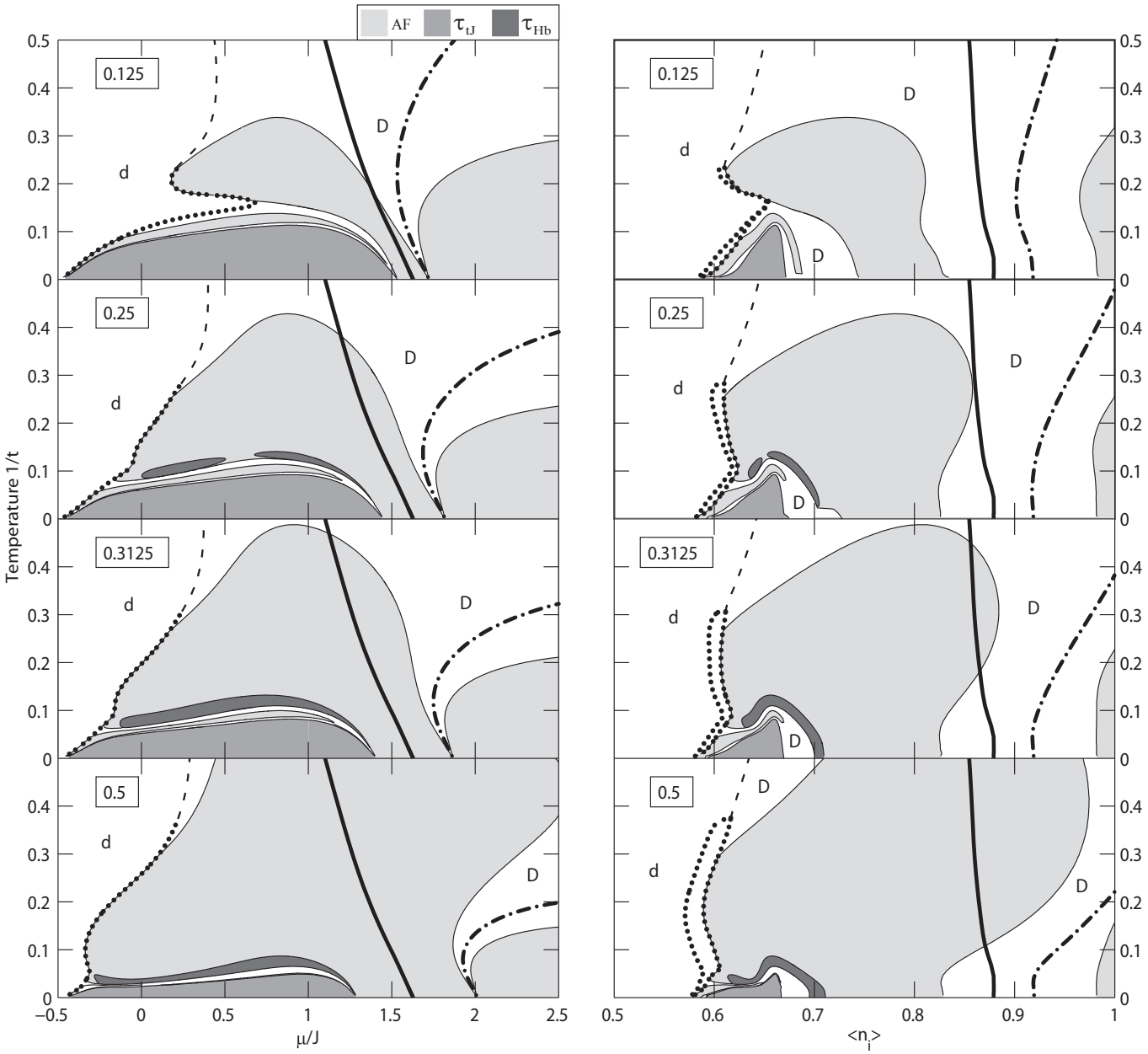

FIG. 5: The continuation of the global phase diagrams in Fig. 4.

Figs. 2 and 3 give the global phase diagram of the t_2 model, as a function of temperature, electron density, chemical potential, and t_2/t. The values of the hopping-strength ratios t_2/t for the consecutive panels in these figures are chosen so that they sequentially produce the qualitatively different phase-diagram cross-sections, thereby revealing the evolution in the global phase diagram. Second-order phase transitions are drawn with full curves, first-order transitions with dotted curves. Phase separation occurs between the dense (D) and dilute (d) disordered phases, in the unmarked areas within the dotted curves in the electron density vs. temperature diagrams. These areas are bounded, on the right and and the left, by the two branches of phase separation densities, evaluated by renormalization-group theory as explained in Sec.IIIC. Note that these coexistence regions between dense (D) and dilute (d) disordered phases are very narrow.

The cross-section $t_2 = 0$ is the phase diagram obtained in previous work [5]. This diagram contains the τ_{tJ} phase between $33 - 37\%$ hole doping away from half-filling and at temperatures $1/t < 0.12$. The thick full curve here gives the systems devoid of electron hopping due to the combined effects of temperature and doping on a nearest-neighbor-only interaction system. The first term of Eq. (18) is positive on the high density/chemical

potential, low temperature side of the thick full curve and negative on the low chemical potential/density, high temperature side of the thick full curve. Thus, the inclusion of $t_2 > 0$ will create competition and frustration (respectively reducing and eliminating the τ phases) on the low chemical potential/density, high temperature side of the curve discussed here, reinforcement (enhancing the τ phases) on the high chemical potential/density, low temperature side of the same curve. The opposite occurs at $t_2 < 0$. The thick full (no-hopping) curve of $t_2 = 0$ is included, again as thick and full, in the $t_2 \neq 0$ phase diagrams and the effects discussed here are seen in the evolution, in both directions, of the global phase diagram.

Pursuing the negative values of t_2, we see at $t_2/t = -0.0625$ that the τ_{tJ} phase, being below the thick full curve, is indeed reduced and bisected into two disconnected regions by the frustration (dash-dotted) curve. At the more negative value of t_2/t = -0.125, only the higher doping region of the τ_{tJ} phase remains and is enhanced as explained after Eq. (18), extending through a wider range to $45 - 55\%$ hole doping. The antiferromagnetic and disordered phases take part in a complex lamellar structure, in a narrow band between $35 - 45\%$ hole doping at low temperatures. At the even more negative values of $t_2/t = -0.25$ and -0.5, the τ_{tJ} phase appears in a wide range of hole doping, between $35 - 55\%$. Besides the complex lamellar structure of antiferromagnetic and disordered phases, we also see that the τ_{Hb} phase participates in the lamellar phase structure and, separately, appears adjacently to the antiferromagnetic phase near half-filling. Particularly near half-filling, the τ_{Hb} phase which evolves adjacently to the antiferromagnetic phase reaches to the higher temperatures of $1/t \sim 0.5$. This topology is identical to that obtained for the Hubbard model [4].

For the positive values of t_2/t, the τ phases are enhanced as explained after Eq. (18) and the topology quickly evolves to that encountered in the Hubbard model. The τ_{tJ} is not bisected by the frustration (dash-dotted) curve and appears between $33 - 37\%$ hole doping as a continuation of the structure at $t_2 = 0$. The τ_{Hb} phase occurs again in two distinct regions and the one which lies nearer to half-filling again extends to high temperatures.

B. The J_2 Model

The J_2 model includes further-neighbor antiferromagnetic interaction, as shown in Fig. 1. The three-site Hamiltonian, between the lattice nodes at the lowest length scale, has the form:

$$-\beta H(i,j,k) = -\beta H(i,j) - \beta H(j,k) - J_2 \sum_{\langle ik \rangle} \mathbf{S}_i \cdot \mathbf{S}_k \,, \tag{20}$$

where $-\beta H(i,j)$ is given in Eq. (2), so that the second equation of Eq. (7) gets modified as

$$J' = \ln \frac{\gamma_6}{\gamma_7} + J_2 \,, \tag{21}$$

only for the first renormalization. Thus, for $d = 3$, the second equation of Eq. (11) gets modified as

$$J' = 4 \ln \frac{\gamma_6}{\gamma_7} + 4\, J_2 \,, \tag{22}$$

only for the first renormalization. Again, the interaction J_2 contributes to the first renormalization, but is not regenerated by this first renormalization. Reinforcement or competition occurs when J_2 is, respectively, of same or opposite sign as the first term in Eq. (22). These two regimes are again separated by the thick full lines in the phase diagrams of Figs. 3 and 4, while again frustration occurs on the dash-dotted lines. In the reinforcement regime, we expect a large extent of the antiferromagnetic phase. The τ_{Hb} phase is also expected to grow in the reinforced region, for it is found along the temperature extent of the antiferromagnetic phase.

Figs. 4 and 5 show the global phase diagram of the J_2 model, as a function of temperature, electron density, chemical potential, and J_2/J. Again, the values of the coupling-strength ratios J_2/J for the consecutive panels in these figures are chosen so that they sequentially produce the qualitatively different phase-diagram cross-sections, thereby revealing the evolution in the global phase diagram. Again, the phase separation regions of the first-order phase transitions are very narrow. For negative values of J_2/J, the antiferromagnetic phase is enhanced, both near half-filling by the mechanism explained after Eq. (22) and, separately and to a lesser extent, displacing the τ_{tJ} phase. The latter behavior is similar to that seen under the introduction of quenched impurities, both experimentally [34–36] and from renormalization-group theory [7]. The τ_{Hb} phase improves near the large antiferromagnetic region near half-filling. At $J_2/J = -2$, the τ_{Hb} phase is found in a wide range of hole doping, namely between $15 - 30\%$. Another interesting result is that the τ_{tJ} phase is depressed in temperature but remains stable in the interval of $33 - 37\%$ hole doping.

For positive values of J_2/J, the antiferromagnetic phase is reduced in the region near half-filling and enhanced in the region near the τ_{tJ} phase, for reasons explained after Eq. (22). The τ_{Hb} phase grows adjacently to the enhanced antiferromagnetic region, being located above the τ_{tJ} phase, causing a complex structure at higher hole dopings and low temperatures.

C. Conclusion

We have shown that the tJ model with further-neighbor antiferromagnetic (J_2) or further-neighbor electron hopping (t_2) interactions exhibits extremely rich

global phase diagrams. The phase separation regions of the first-order phase transions are very narrow. Furthermore, these calculated phase diagrams are understood in terms of the competition and frustration of nearest- and further-neighbor interactions. We find that the two types of τ phases, previously seen in the Hubbard model, occur in the tJ model with the inclusion of further-neighbor interactions.

Acknowledgments

This research was supported by the Scientific and Technological Research Council of Turkey (TÜBİTAK) and by the Academy of Sciences of Turkey.

n	p	s	m_s	Two-site eigenstates
0	+	0	0	$\|\phi_1\rangle = \|\circ\,\circ\rangle$
1	+	1/2	1/2	$\|\phi_2\rangle = \frac{1}{\sqrt{2}}\{\|\uparrow\circ\rangle + \|\circ\uparrow\rangle\}$
1	−	1/2	1/2	$\|\phi_4\rangle = \frac{1}{\sqrt{2}}\{\|\uparrow\circ\rangle - \|\circ\uparrow\rangle\}$
2	−	0	0	$\|\phi_6\rangle = \frac{1}{\sqrt{2}}\{\|\uparrow\downarrow\rangle - \|\downarrow\uparrow\rangle\}$
2	+	1	1	$\|\phi_7\rangle = \|\uparrow\uparrow\rangle$
2	+	1	0	$\|\phi_9\rangle = \frac{1}{\sqrt{2}}\{\|\uparrow\downarrow\rangle + \|\downarrow\uparrow\rangle\}$

TABLE III: The two-site basis states, with the corresponding particle number (n), parity (p), total spin (s), and total spin z-component (m_s) quantum numbers. The states $|\phi_3\rangle$, $|\phi_5\rangle$, and $|\phi_8\rangle$ are obtained by spin reversal from $|\phi_2\rangle$, $|\phi_4\rangle$, and $|\phi_7\rangle$, respectively.

Appendix A: Derivation of the Decimation Relations

The derivation of Eq. (7), first done in Ref.[5], is given in this Appendix. In Eq. (5) the operators $-\beta' H'(i,k)$ and $-\beta H(i,j) - \beta H(j,k)$ act on two-site and three-site states, respectively, where at each site an electron may be either with spin $\sigma =\uparrow$ or $\downarrow$, or may not exist (0 state). In terms of matrix elements,

$$\langle u_i v_k|e^{-\beta' H'(i,k)}|\bar{u}_i\bar{v}_k\rangle = \sum_{w_j}\langle u_i\, w_j\, v_k|e^{-\beta H(i,j)-\beta H(j,k)}|\bar{u}_i\, w_j\, \bar{v}_k\rangle\,, \quad \text{(A1)}$$

where $u_i, w_j, v_k, \bar{u}_i, \bar{v}_k$ are single-site state variables, so that the left-hand side reflects a 9×9 and the right-hand side a 27×27 matrix. Basis states that are simultaneous eigenstates of total particle number (n), parity (p), total spin magnitude (s), and total spin z-component (m_s) block-diagonalize Eq. (A1) and thereby make it manageable. These sets of 9 two-site and 27 three-site eigenstates, denoted by $\{|\phi_p\rangle\}$ and $\{|\psi_q\rangle\}$ respectively, are given in Tables III and IV. Eq. (A1) is thus rewritten as

n	p	s	m_s	Three-site eigenstates
0	+	0	0	$\|\psi_1\rangle = \|\circ\,\circ\,\circ\rangle$
1	+	1/2	1/2	$\|\psi_2\rangle = \|\circ\uparrow\circ\rangle$, $\|\psi_3\rangle = \frac{1}{\sqrt{2}}\{\|\uparrow\circ\,\circ\rangle + \|\circ\,\circ\uparrow\rangle\}$
1	−	1/2	1/2	$\|\psi_6\rangle = \frac{1}{\sqrt{2}}\{\|\uparrow\circ\,\circ\rangle - \|\circ\,\circ\uparrow\rangle\}$
2	+	0	0	$\|\psi_8\rangle = \frac{1}{2}\{\|\uparrow\downarrow\circ\rangle - \|\downarrow\uparrow\circ\rangle - \|\circ\uparrow\downarrow\rangle + \|\circ\downarrow\uparrow\rangle\}$
2	−	0	0	$\|\psi_9\rangle = \frac{1}{2}\{\|\uparrow\downarrow\circ\rangle - \|\downarrow\uparrow\circ\rangle + \|\circ\uparrow\downarrow\rangle - \|\circ\downarrow\uparrow\rangle\}$, $\|\psi_{10}\rangle = \frac{1}{\sqrt{2}}\{\|\uparrow\circ\downarrow\rangle - \|\downarrow\circ\uparrow\rangle\}$
2	+	1	1	$\|\psi_{11}\rangle = \|\uparrow\circ\uparrow\rangle$, $\|\psi_{12}\rangle = \frac{1}{\sqrt{2}}\{\|\uparrow\uparrow\circ\rangle + \|\circ\uparrow\uparrow\rangle\}$
2	+	1	0	$\|\psi_{13}\rangle = \frac{1}{2}\{\|\uparrow\downarrow\circ\rangle + \|\downarrow\uparrow\circ\rangle + \|\circ\uparrow\downarrow\rangle + \|\circ\downarrow\uparrow\rangle\}$, $\|\psi_{14}\rangle = \frac{1}{\sqrt{2}}\{\|\uparrow\circ\downarrow\rangle + \|\downarrow\circ\uparrow\rangle\}$
2	−	1	1	$\|\psi_{17}\rangle = \frac{1}{\sqrt{2}}\{\|\uparrow\uparrow\circ\rangle - \|\circ\uparrow\uparrow\rangle\}$
2	−	1	0	$\|\psi_{18}\rangle = \frac{1}{2}\{\|\uparrow\downarrow\circ\rangle + \|\downarrow\uparrow\circ\rangle - \|\circ\uparrow\downarrow\rangle - \|\circ\downarrow\uparrow\rangle\}$
3	+	1/2	1/2	$\|\psi_{20}\rangle = \frac{1}{\sqrt{6}}\{2\|\uparrow\downarrow\uparrow\rangle - \|\uparrow\uparrow\downarrow\rangle - \|\downarrow\uparrow\uparrow\rangle\}$
3	−	1/2	1/2	$\|\psi_{22}\rangle = \frac{1}{\sqrt{2}}\{\|\uparrow\uparrow\downarrow\rangle - \|\downarrow\uparrow\uparrow\rangle\}$
3	+	3/2	3/2	$\|\psi_{24}\rangle = \|\uparrow\uparrow\uparrow\rangle$
3	+	3/2	1/2	$\|\psi_{25}\rangle = \frac{1}{\sqrt{3}}\{\|\uparrow\downarrow\uparrow\rangle + \|\uparrow\uparrow\downarrow\rangle + \|\downarrow\uparrow\uparrow\rangle\}$

TABLE IV: The three-site basis states, with the corresponding particle number (n), parity (p), total spin (s), and total spin z-component (m_s) quantum numbers. The states $|\psi_{4-5}\rangle$, $|\psi_7\rangle$, $|\psi_{15-16}\rangle$, $|\psi_{19}\rangle$, $|\psi_{21}\rangle$, $|\psi_{23}\rangle$, $|\psi_{26-27}\rangle$ are obtained by spin reversal from $|\psi_{2-3}\rangle$, $|\psi_6\rangle$, $|\psi_{11-12}\rangle$, $|\psi_{17}\rangle$, $|\psi_{20}\rangle$, $|\psi_{22}\rangle$, $|\psi_{24-25}\rangle$, respectively.

	ϕ_1	ϕ_2	ϕ_4	ϕ_6	ϕ_7	ϕ_9
ϕ_1	G'					
ϕ_2		$-t'+\mu'+G'$		0		
ϕ_4			$t'+\mu'+G'$			
ϕ_6				$\frac{3}{4}J'+V'+2\mu'+G'$		
ϕ_7			0		$-\frac{1}{4}J'+V'+2\mu'+G'$	
ϕ_9						$-\frac{1}{4}J'+V'+2\mu'+G'$

TABLE V: Block-diagonal matrix of the renormalized two-site Hamiltonian $-\beta' H'(i,k)$. The Hamiltonian being invariant under spin-reversal, the spin-flipped matrix elements are not shown.

$$\langle\phi_p|e^{-\beta' H'(i,k)}|\phi_{\bar{p}}\rangle = \sum_{\substack{u,v,\bar{u},\\ \bar{v},w}}\sum_{q,\bar{q}}\langle\phi_p|u_i v_k\rangle\langle u_i w_j v_k|\psi_q\rangle\langle\psi_q|e^{-\beta H(i,j)-\beta H(j,k)}|\psi_{\bar{q}}\rangle\cdot \langle\psi_{\bar{q}}|\bar{u}_i w_j\bar{v}_k\rangle\langle\bar{u}_i\bar{v}_k|\phi_{\bar{p}}\rangle\,. \quad \text{(A2)}$$

There are five independent elements for $\langle\phi_p|e^{-\beta' H'(i,k)}|\phi_{\bar{p}}\rangle$ in Eq.(A2) (thereby leading to five renormalized interaction constants $\{t', J', V', \mu', G'\}$),

	ψ_1
ψ_1	0

	ψ_2	ψ_3
ψ_2	2μ	$-\sqrt{2}t$
ψ_3	$-\sqrt{2}t$	μ

	ψ_6	ψ_8
ψ_6	μ	0
ψ_8	0	$\frac{3}{4}J+V+3\mu$

	ψ_9	ψ_{10}
ψ_9	$\frac{3}{4}J+V+3\mu$	$-\sqrt{2}t$
ψ_{10}	$-\sqrt{2}t$	2μ

	ψ_{11}	ψ_{12}
ψ_{11}	2μ	$-\sqrt{2}t$
ψ_{12}	$-\sqrt{2}t$	$-\frac{1}{4}J+V+3\mu$

	ψ_{13}	ψ_{14}
ψ_{13}	$-\frac{1}{4}J+V+3\mu$	$-\sqrt{2}t$
ψ_{14}	$-\sqrt{2}t$	2μ

	ψ_{17}	ψ_{18}
ψ_{17}	$-\frac{1}{4}J+V+3\mu$	0
ψ_{18}	0	$-\frac{1}{4}J+V+3\mu$

	ψ_{20}
ψ_{20}	$J+2V+4\mu$

	ψ_{22}
ψ_{22}	$2V+4\mu$

	ψ_{24}
ψ_{24}	$-\frac{1}{2}J+2V+4\mu$

	ψ_{25}
ψ_{25}	$-\frac{1}{2}J+2V+4\mu$

TABLE VI: Diagonal matrix blocks of the unrenormalized three-site Hamiltonian $-\beta H(i,j)-\beta H(j,k)$. The Hamiltonian being invariant under spin-reversal, the spin-flipped matrix elements are not shown.

which we label γ_p,

$$\gamma_p \equiv \langle\phi_p|e^{-\beta' H'(i,k)}|\phi_p\rangle \quad \text{for } p=1,2,4,6,7\,. \tag{A3}$$

The diagonal matrix $\langle\phi_p|-\beta' H'(i,k)|\phi_{\bar{p}}\rangle$ is given in Table V. The exponential of this matrix yields the five renormalized interaction constants in terms of γ_p, as given in Eq. (7). Furthermore, according to Eq. (A2), each γ_p is a linear combination of some $\langle\psi_q|e^{-\beta H(i,j)-\beta H(j,k)}|\psi_{\bar{q}}\rangle$,

$$\gamma_1 = \langle\psi_1||\psi_1\rangle+\langle\psi_2||\psi_2\rangle+\langle\psi_4||\psi_4\rangle\,,$$

$$\gamma_2 = \langle\psi_3||\psi_3\rangle+\frac{1}{2}\langle\psi_8||\psi_8\rangle+\langle\psi_{12}||\psi_{12}\rangle+\frac{1}{2}\langle\psi_{13}||\psi_{13}\rangle\,,$$

$$\gamma_4 = \langle\psi_6||\psi_6\rangle+\frac{1}{2}\langle\psi_9||\psi_9\rangle+\langle\psi_{17}||\psi_{17}\rangle+\frac{1}{2}\langle\psi_{18}||\psi_{18}\rangle\,,$$

$$\gamma_6 = \langle\psi_{10}||\psi_{10}\rangle+2\langle\psi_{22}||\psi_{22}\rangle\,,$$

$$\gamma_7 = \langle\psi_{11}||\psi_{11}\rangle+\frac{2}{3}\langle\psi_{20}||\psi_{20}\rangle+\frac{4}{3}\langle\psi_{24}||\psi_{24}\rangle\,,$$

where $\langle\psi_q||\psi_q\rangle \equiv \langle\psi_q|e^{-\beta H(i,j)-\beta H(j,k)}|\psi_q\rangle$. In order to calculate $\langle\psi_q|e^{-\beta H(i,j)-\beta H(j,k)}|\psi_{\bar{q}}\rangle$ the matrix blocks in Table VI are numerically exponentiated.

[1] J. Hubbard, Proc. R. Soc. A **276**, 238 (1963); **277**, 237 (1964); **281**, 401 (1964).
[2] P.W. Anderson, Science **235**, 1196 (1987).
[3] G. Baskaran, Z. Zhou, and P.W. Anderson, Solid State Commun. **63**, 973 (1987).
[4] M. Hinczewski and A.N. Berker, Eur. Phys. J. B **48**, 1 (2005).
[5] A. Falicov and A.N. Berker, Phys. Rev. B **51**, 12458 (1995).
[6] M. Hinczewski and A.N. Berker, Eur. Phys. J. B **51**, 461 (2006).
[7] M. Hinczewski and A.N. Berker, Phys. Rev. B **78**, 064507 (2008).
[8] A.V. Puchkov, P. Fournier, T. Timusk, and N.N. Kolesnikov, Phys. Rev. Lett. **77**, 1853 (1996).
[9] C. Bernhard, J.L. Tallon, T. Blasius, A. Golnik, and C. Niedermayer, Phys. Rev. Lett. **86**, 1614 (2001).
[10] G. Jüttner, A. Klümper, and J. Suzuki, Nucl. Phys. B **522**, 471 (1998).
[11] G. Jüttner, A. Klümper, and J. Suzuki, Physica B **259-261**, 1019 (1999).
[12] M. Hinczewski, Ph.D. Thesis, Massachusetts Institute of Technology, Chap. 2 (2005), http://dspace.mit.edu/handle/1721.1/34392.
[13] M. Ogata, M.U. Luchini, S. Sorella, and F.F. Assaad, Phys. Rev. Lett. **66**, 2388 (1991).
[14] S. Krinsky and D. Furman, Phys. Rev. Lett. **32**, 731 (1974).
[15] S. Krinsky and D. Furman, Phys. Rev. B **11**, 2602 (1975).
[16] S.A. Kivelson, V.J. Emery, and H.Q. Lin, Phys. Rev. B **42**, 6523 (1990).
[17] W.O. Putikka, M.U. Luchini, and T.M. Rice, Phys. Rev. Lett. **68**, 538 (1992).
[18] E. Dagotto, Rev. Mod. Phys. **66**, 763 (1994)
[19] M. Suzuki and H. Takano, Phys. Lett. A **69**, 426 (1979).
[20] H. Takano and M. Suzuki, J. Stat. Phys. **26**, 635 (1981).
[21] P. Tomczak, Phys. Rev. B **53**, R500 (1996).
[22] P. Tomczak and J. Richter, Phys. Rev. B **54**, 9004 (1996).
[23] P. Tomczak and J. Richter, J. Phys. A **36**, 5399 (20 03).
[24] C.N. Kaplan and A.N. Berker, Phys. Rev. Lett. **100**, 027204 (2008).
[25] O.S. Sarıyer, A.N. Berker, and M. Hinczewski, Phys. Rev. B **77**, 134413 (2008).
[26] A.A. Migdal, Zh. Eksp. Teor. Fiz. **69**, 1457 (1975) [Sov. Phys. JETP **42**, 743 (1976)].
[27] L.P. Kadanoff, Ann. Phys. (N.Y.) **100**, 359 (1976).
[28] A.N. Berker and M. Wortis, Phys. Rev. B **14**, 4946 (1976).
[29] S.R. McKay and A.N. Berker, Phys. Rev. B **29**, 1315 (1984).
[30] M.E. Fisher and A.N. Berker, Phys. Rev. B **26**, 2507 (1982).
[31] A.N. Berker, S. Ostlund, and F.A. Putnam, Phys. Rev. B **17**, 3650 (1978).
[32] R.G. Caflisch and A.N. Berker, Phys. Rev. B **29**, 1279 (1984).
[33] R.G. Caflisch, A.N. Berker, and M. Kardar, Phys. Rev. B **31**, 4527 (1985).
[34] M.-H. Julien, T. Fehér, M. Horvatić, C. Berthier, O.N. Bakharev, P. Ségransan, G. Collin, and J.-F. Marucco,

Phys. Rev. Lett. **84**, 3422, (2000).
[35] I. Watanabe, T. Adachi, K. Takahashi, S. Yairi, Y. Koike, and K. Nagamine, Phys. Rev. B **65**, 180516(R) (2002).
[36] Y. Itoh, T. Machi, C. Kasai, S. Adachi, N. Watanabe, N. Koshizuka, and M. Murakami, Phys. Rev. B **67**, 064516 (2003).